2024 IEEE International Conference on Robotics and Automation (ICRA 2024)
May 13-17, 2024. Yokohama, Japan

Vision-Based Water Clearance Determination in Maritime Environment

Carl H. Schiller* Deran Maas* Bruno Arsenali* Jukka Peltola** Kalevi Tervo** Stefano Maranò*

***Abstract*— Determining the distances from the hull of the own ship to obstacles or land, i.e. water clearance, is a fundamental task in navigation. This is particularly relevant during maneuvering in the harbor or navigating in confined waters. We introduce the concepts of area water clearance and line water clearance. Area water clearance is important especially for path planning and obstacle avoidance. Line water clearance is critical for maneuvering when approaching the quay.**

In this work, we present a vision-based approach to determine the water clearance. A single calibrated camera together with a semantic segmentation network is used to detect the water region in an image, and back-projection to determine the water clearance on the sea surface in world units.

We validate the proposed approach on real data collected from two distinct vessels, where the proposed method is able to produce reliable water clearance for distances beyond one kilometer. During harbor maneuvering 90% of the relative water clearance errors were found to be between -2.3% and 3%.

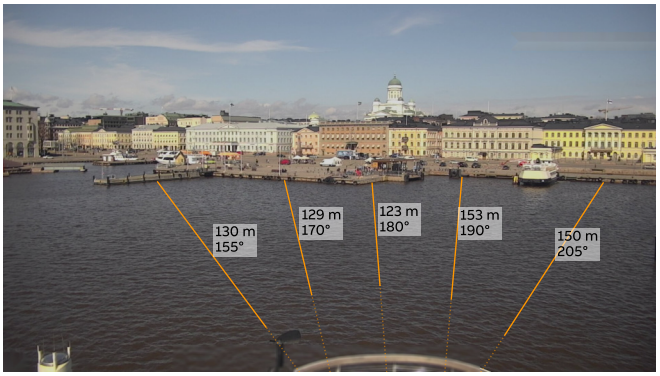

Fig. 1: Suomenlinna II approaching Kauppatori Market Square in Helsinki. The orange lines depict the water clearance computed from different points from the ship's hull to the first obstacle along different bearings.

I. INTRODUCTION

An important task, vital to safe navigation, is the determination of water clearance, i.e., estimating the distances from the hull of the own ship to obstacles or land. This is particularly relevant during maneuvering in the harbor when distances from hull to the quay walls need to be known. During navigation, it is similarly necessary to continuously monitor the water clearance between the hull and, for example, navigational aid poles, buoys, emerged land, or any floating objects. Fig. 1 depicts an image captured from the lookout camera of a ferry approaching a quay, where water clearance distances are computed using the proposed method from the ship's hull along several pre-defined bearings.

Depending on ship size and maneuverability, water clearances may need to be known from several hundred meters down to tens of centimeters away from obstacles. Different solutions are used for this purpose. Relying on the position estimate for the ego-vessel provided by global navigation satellite system (GNSS) and navigational charts may be a viable solution for large distances down to a few meters. However, loss of GNSS would leave the ship without vital information and, depending on the frequency and precision of survey data, charts can vary greatly in their accuracy.

Light detection and ranging (LiDAR) has also been used to determine the distance to quay structures. While LiDARs are known to be accurate sensors, the applicability is limited to the range of the sensors, which may not exceed few hundred meters.

Authors are with: * ABB Corporate Research, Baden-Dättwil, Switzerland; ** ABB Marine & Ports, Helsinki, Finland. Corresponding author email: stefano.marano@ch.abb.com

Lastly, it is not uncommon to estimate water clearance based on visual assessments of the crew. This method is clearly prone to very subjective measurements.

In this work, we propose a monocular vision system to determine water clearance based on an image captured by a calibrated onboard camera. We use semantic segmentation to determine the water pixels in the image. An onboard inertial measurement unit (IMU) is used to adjust the camera pose, semantic information is back-projected on the sea surface, and clearance to obstacles are computed in world units. A vision-based water clearance method may complement or replace other technologies, depending on the application. Cameras work for both large and short ranges, do not rely on external information sources such as charts, and can identify unexpected objects in the field of view (FOV). Additionally, the cost of cameras make them significantly more economical compared to other sensing modalities.

This work focuses on two main contributions. First, the determination of *area water clearance* as a two-dimensional map and the calculation of *water clearance distances* along predefined lines. Second, validating the estimated water clearance distances with a ground truth obtained from coastline charts and GNSS. A similar vision-based approach has been used in [1] to determine the navigable area in the FOV of a camera for the purpose of path planning without evaluation of the quality of the navigable area.

The rest of this manuscript is organized as follows. Sec. II summarizes previous related work. Sec. III describes the proposed method. The validation method and results are presented in Sec. IV. Conclusions are drawn Sec. V.

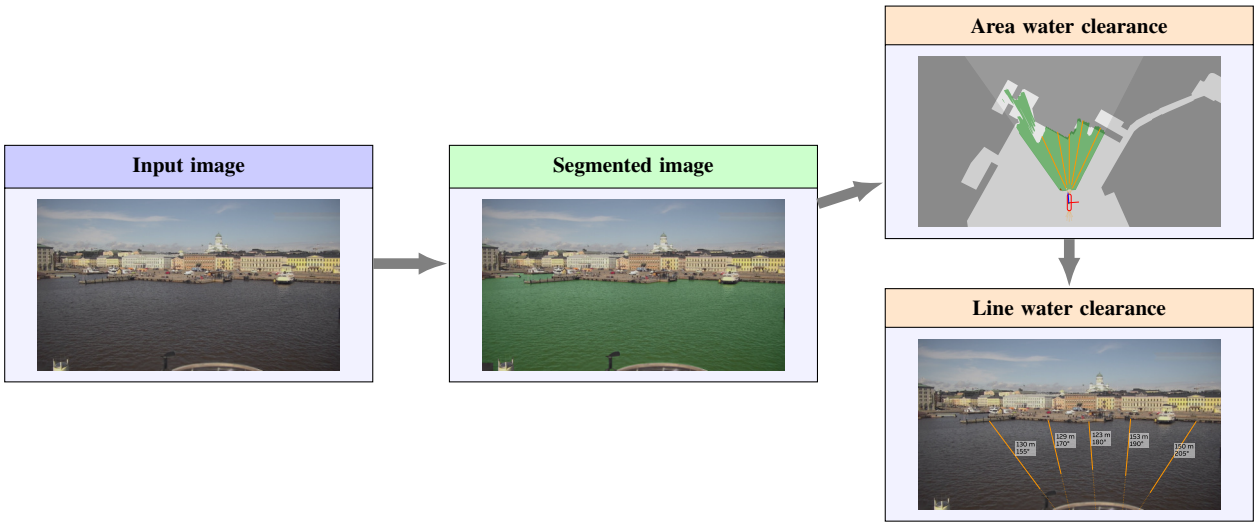

Fig. 2: Overview of proposed method. The input image is semantically segmented producing regions of water and non-water. Polygons describing the water region on the image are extracted and are projected on the sea plane. The area water clearance is shown in green and is available within the camera FOV. Lastly, the line water clearances and the distances up to the first obstacles are computed.

II. RELATED WORK

Determination of water clearances for maritime applications has been investigated in recent literature. Some works focus on the detection of obstacles such as other vessels, while others focus on the determination of the navigable area.

Several authors employ a stereo-vision system to detect and locate obstacles on the sea surface [2], [3], [4], [5]. In [5], the authors rely on semantic segmentation to detect obstacles on the sea surface, and IMU is used to constrain the segmentation, finally camera pairs are used to verify the detections.

Other authors have used radar for similar purposes. In [6], a convolutional neural network (CNN) algorithm is used for semantic segmentation of land and floating objects from marine radar images. In [7], camera images are used together with handcrafted radar features to segment the water on inland waterways.

LiDAR as a sensing modality has also been the focus of several works in recent years. In [8], the navigable region is determined using LiDAR, where point clouds are segmented into river banks, bridges and vegetation. The detected river banks are tracked over subsequent LiDAR scans and the navigable region is then determined with a wave frontier detection method [9].

In [1], navigable regions are found using both LiDAR and a single camera. The navigable region is is used for planning the path of a surface vessel. Water in images is detected with a segmentation network, the water region is transformed from image to world coordinates. From the water region in world coordinates, a set of points of navigable boundary points are extracted. The LiDAR point cloud is processed using the Hough transform to detect vertical walls. A combination of vision-based boundary points and LiDAR-based walls are used as input for a trajectory optimization algorithm. However, [1] does not provide an analysis of the accuracy of the estimated navigable region, which will be the focus of this work using a similar approach.

Segmentation of the water region from marine images has been presented in multiple works. Semantic segmentation using CNN is a common and successful approach. Obstacle and water detection for marine applications has been evaluated in [10], [11], [12] using object detection and/or semantic segmentation. In these work the evaluation is limited to the image-space.

Our work is the first to focus on the water clearance distance computation from the area water clearance and is the first to show an extensive validation on real data.

III. METHOD

The proposed method relies on a single camera mounted onboard of the ego-vessel, that is positioned and oriented to capture a region of interest containing a water region and eventual obstacles. Using a CNN the images taken by the camera are semantically segmented to predict regions of water. Water regions are back-projected from the image plane onto the sea surface, determining the area water clearance. In a last step, water clearance distances between the hull of the ego-vessel and the first obstacle are determined from the area clearance. A schematic representation of the proposed method is shown in Figure 2.

A. Semantic segmentation

We use a pre-trained MobileNetV2 [13] as backbone feature extractor. It is primarily designed for mobile devices, and hence is computationally lightweight. Furthermore, we extend the feature extractor with a U-Net type decoder [14], which is a well known CNN for fast and precise segmentation of images. The output of the proposed architecture is a

three-dimensional matrix, containing the predicted probabilities that a pixel from the input image belongs to a certain class, i.e., water and non-water. Cross entropy loss is used to train the network.

B. Coordinate transformations and IMU correction

We consider four coordinate systems to describe how pixels on the image relate to the ego-vessel and the sea surface. Namely, the image $\{\mathrm{i}\}$, the camera $\{\mathrm{c}\}$, the vessel $\{\mathrm{v}\}$, and the sea-keeping $\{\mathrm{s}\}$ coordinate systems.

The vessel coordinate system $\{\mathrm{v}\}$ is attached to the vessel. In absence of pitching and rolling, $\{\mathrm{s}\}$ coincides with $\{\mathrm{v}\}$. The xy-plane of $\{\mathrm{v}\}$ coincides with the sea surface and the z-axis points up. Any perturbation to either roll or pitch makes the vessel rotate about its equilibrium causes $\{\mathrm{v}\}$ to move accordingly while $\{\mathrm{s}\}$ remains attached to the resting orientation of the vessel. In our model, the sea-keeping coordinate system $\{\mathrm{s}\}$ and vessel coordinate system $\{\mathrm{v}\}$ are solely related by rolling and pitching rotations. The coordinate transformation from $\{\mathrm{v}\}$ to $\{\mathrm{s}\}$ is described by the matrix $R \in SE(3)$, which accounts for the current pitch and roll of the vessel provided by an onboard IMU. Since the position and orientation of the camera in relation to the ship is known, the *extrinsic camera matrix* is easily formed and combined with R, which results in the total transformation $T \in SE(3)$ from $\{\mathrm{c}\}$ to $\{\mathrm{s}\}$.

A pinhole camera model [15] is used to map coordinates in $\{\mathrm{c}\}$ onto the two-dimensional image coordinate system $\{\mathrm{i}\}$. Let K be the 3×4 matrix

$$K := \begin{bmatrix} f_x & 0 & x_0 & 0 \\ 0 & f_y & y_0 & 0 \\ 0 & 0 & 1 & 0 \end{bmatrix} \tag{1}$$

where f_x, f_y are the focal lengths and x_0, y_0 are the principal point offsets. The matrix K is referred to as the *intrinsic camera matrix*. By combining the previously mentioned IMU corrected T with K, the total transform from $\{\mathrm{s}\}$ to $\{\mathrm{i}\}$ is KT. In this work, the inverse transform onto the sea surface in $\{\mathrm{s}\}$ is of interest. Hence, the image coordinates (u, v)

$$\begin{bmatrix} u \\ v \\ 1 \end{bmatrix} = KT \begin{bmatrix} x \\ y \\ 0 \\ 1 \end{bmatrix} \tag{2}$$

are used to solve for (x, y) in $\{\mathrm{s}\}$. This inverse transformation is conventionally called *back-projection*.

C. Area water clearance

The area (water) clearance correspond to the sea surface within the FOV of the camera that is free of obstacles. This area is relevant, for example, in the planning of the path of the ego-vessel.

To determine the area clearance the segmented water region in the image is back-projected on the sea surface and the area clearance is determined in the sea-keeping reference frame $\{\mathrm{s}\}$. The output of the segmentation network described in III-A is converted into a binary image representing detected water and non-water pixels by selecting the predicted class with the highest probability. Using the contour detection algorithm [16], a set of polygons $\mathcal{W}_{\{i\}}$ representing regions containing predicted water is extracted from the binary image. Using back-projection described in (2) the polygon set $\mathcal{W}_{\{i\}}$ is transformed in the sea-keeping frame $\{\mathrm{s}\}$ as $\mathcal{W}$.

D. Line water clearance

The line (water) clearance is used to determine the water clearance distance d_w in world units between a starting point and the first obstacle in the area clearance along a pre-defined line. To determine the distance d_w we rely on geometrical operations on the xy-plane of the sea-keeping frame $\{\mathrm{s}\}$, which coincides with the sea surface.

We consider three points on the sea surface, a starting point, a water point, and an end point, $p_s, p_w, p_e \in \mathbb{R}^2$, respectively. The points p_s, p_w are set to define the water clearance line while p_e is determined with the method described in this section. The starting point does not need to be visible in the image, for example it could be a point near the hull of the ego-vessel which may be not visible from the camera. However, the water point p_w needs to be visible in the image and, in order for the distance d_w to be defined, it needs to belong to $\mathcal{W}$.

In order to determine the end point p_e, we first consider the ray from the starting point p_s passing through the water point p_w

$$\mathcal{R} = \{p_s + t\delta \,|\, t \geq 0\}, \tag{3}$$

where $\delta = (p_w - p_s)/\|p_w - p_s\|_2$ is the direction of the ray. Let $\mathcal{R}(t)$ indicate a point on the ray at distance t from the ray's origin p_s.

The end point of the line clearance, corresponding to the first obstacle in the area clearance, is found at a intersection between the boundary of the area clearance and the ray, i.e., $p_e \in \partial\mathcal{W} \cap \mathcal{R}$. Since the ray and the boundary could have multiple intersections, the suitable end point is found solving

$$\begin{aligned} \hat{d}_w = & \min_d d \\ \text{s.t.} \quad & d > \|p_s - p_w\|_2 \\ & \mathcal{R}(d) \in \partial\mathcal{W}, \end{aligned} \tag{4}$$

where the end point is $p_e = \mathcal{R}(\hat{d}_w)$. The constraint on d prevents picking any intersection between p_s and p_w.

The water clearance distance is $\hat{d}_w = \|p_e - p_s\|_2$. The described approach requires that $p_w \in \mathcal{W}$ and only checks the water clearance between p_w and p_e, assuming that there is no obstacle between p_s and p_w.

IV. RESULTS

In this section we show a quantitative evaluation of the proposed method on two vessels: Suomenlinna II and m/s Finlandia. The estimated water clearance distance from (4) is compared with the ground truth obtained from charts and GNSS-based ego-vessel position.

Suomenlinna II is a passenger ferry operating in Helsinki, Finland. She is 34 m in length and 8 m wide, and is equipped

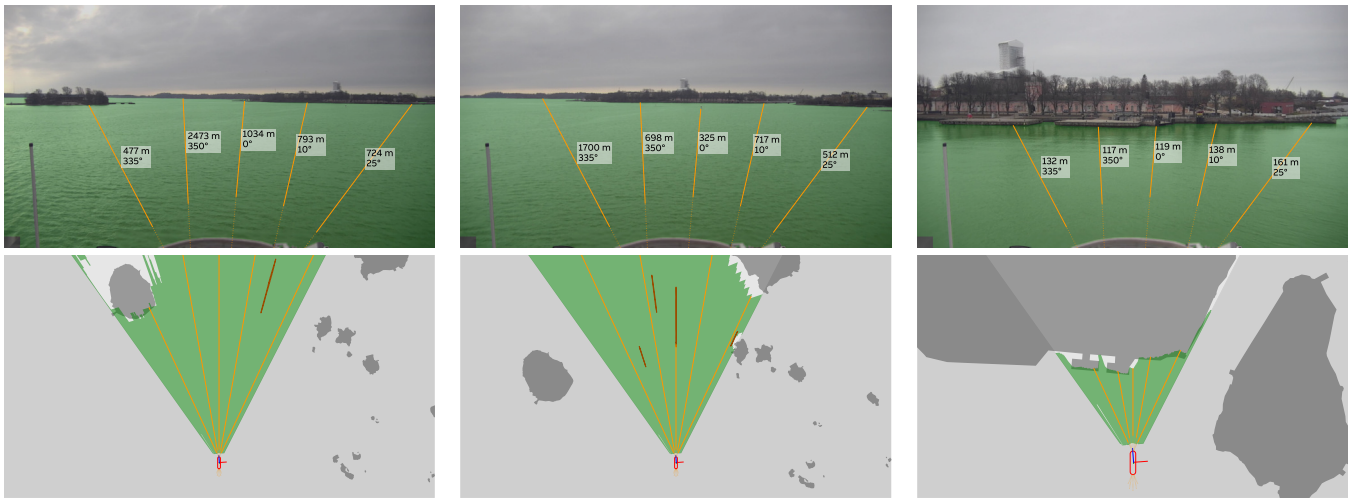

(a) $t = 1\,\mathrm{s}$ (b) $t = 33\,\mathrm{s}$ (c) $t = 176\,\mathrm{s}$

Fig. 3: Images from route Helsinki A.

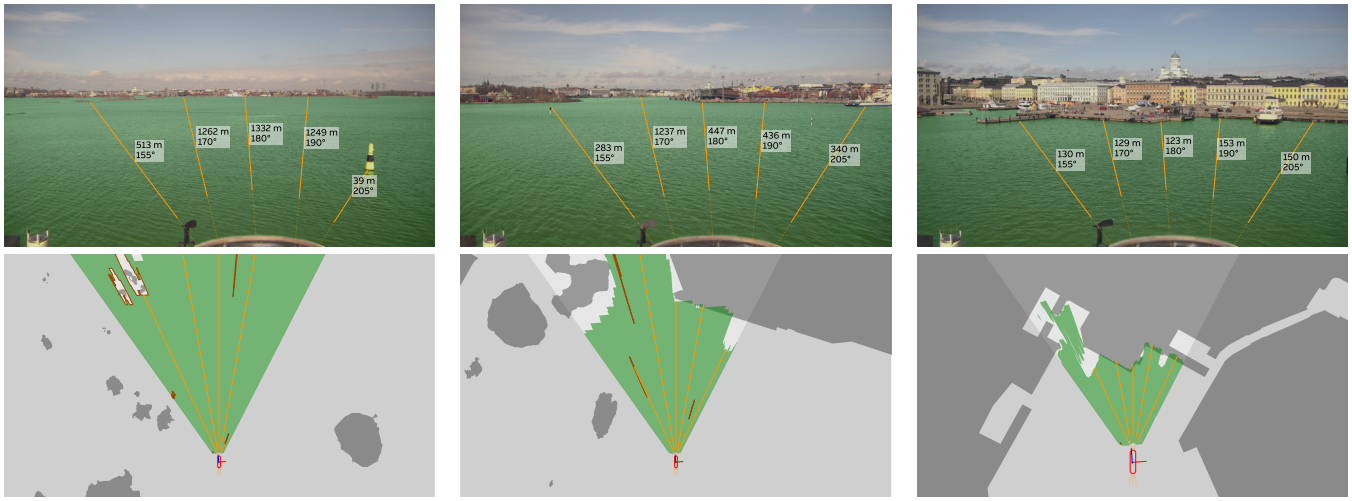

(a) $t = 4\,\mathrm{s}$ (b) $t = 225\,\mathrm{s}$ (c) $t = 500\,\mathrm{s}$

Fig. 4: Images for route Helsinki B.

with a pan-tilt-zoom camera mounted at a height of about 10 m and an onboard IMU. The IMU aided pose correction described in Sec. III-B is performed only for the roll angle.

M/s Finlandia is a roll-on/roll-off passenger ferry operating between Tallinn and Helsinki. She measures 175 m in length and the beam is 27 m. A forward facing camera is mounted at a height of about 30 m. Similarly, an onboard IMU is available and is used to account for both pitch and roll angles.

We note that the heights of the cameras differ significantly between the two vessels. A higher camera is advantageous when observing the water surface. In addition, the different dimensions of the vessels affect the stability, where the larger m/s Finlandia will exhibit smaller rolling and pitching.

Intrinsic camera calibration was performed using a checkerboard and the matrix in (1) is found. The extrinsic parameters were found using a proprietary software relying on comparing projected world landmarks onto the image plane.

The proposed method was tested with 7 fps and runs in real-time on an office workstation. All the processing is performed for each input image individually.

A. *Semantic segmentation*

The network described in Sec. III-A is trained for 200 epochs at a resolution of 960 by 544 pixels and a batch size of four. The dataset is composed of images from a proprietary marine dataset. It contains a mix of onboard and onshore images for a total of about 16000 annotated images. The dataset is split into train and test sets in the ratio of 94/6. To reduce the similarity between train and test sets we pick different operating conditions. After training, the intersection over union (IoU) on the test set for the water class is 0.993.

B. Validation of water clearance distance

To validate the proposed approach, we compare the estimated water clearance distance described in III-D with the ground truth computed from coastline charts. We use the position of the ego-vessel provided by the onboard GNSS and publicly available charts to compute the actual water clearance distance d_w from the hull of the ego-vessel to the coastline. The clearance line along the vessel's centerline is considered in the validation.

We indicate with $\hat{d}_w$ the estimated water clearance distance. We consider the relative error of the distance defined as $(d_w - \hat{d}_w)/d_w$. Due to the projective geometry, errors are expected to be larger for larger distances, hence the relative error is used considered.

This method of evaluation has some limitations. The charts are mostly accurate, but certain quay structures are not present, thus making the ground truth unreliable in certain instances. In addition, some objects such as poles for navigational aid and other vessels, are not present in the coastline charts.

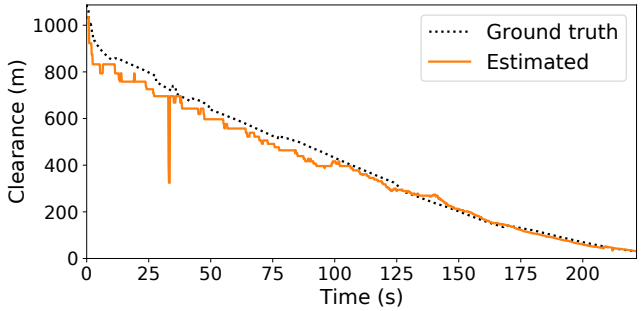

Fig. 5: Water clearance distance for route Helsinki A.

C. Route Helsinki A

In this route, Suomenlinna II is approaching the island of Suomenlinna near Helsinki. In Fig. 3, three camera images along the route are shown together with the corresponding map view. The map view shows in green the segmented water region, possibly with holes corresponding to detected obstacles. Orange lines depict the water clearance lines. The dashed part of each line corresponds to the segment $\overline{p_s p_w}$ where the clearance is assumed, the solid part corresponds to the segment $\overline{p_w p_e}$ where the clearance is checked, cf. Sec. III-D. For each line, the water clearance distance is indicated in meters. The angle correspond to the bearing of the line in vessel coordinates. The map view shows the area water clearance in green and the land in dark gray. Line clearances are also shown in the map view.

Fig. 3a shows the lines reaching land at different distances. In Fig. 3b the line along the centerline, i.e. bearing $0°$ hit a navigation pole over 300 m away. In Fig. 3c the vessel has almost reached the quay and the lines reach the quay structures. Here the area clearance appears to be over-estimated, possibly due to the vessel decelerating causing the bow of the vessel to lower and the lack of pitch compensation.

In Fig. 5 the estimated water clearance distance is compared with the chart-based ground truth. The clearance is estimated from one kilometer until few tens of meters. The water clearance is initially underestimated, the absolute error is reduced as the vessel approaches the harbor. The spike at 33 s is caused by the navigation pole shown in Fig. 3b.

Over the entire path traveled, the median relative error is 6.0%, with 5-th and 95-th percentile errors of -7.3% and 14.1%, respectively. The median relative error may be reduced with better camera calibration. In particular, we believe that the calibration extrinsic of the pan-tilt zoom may be improved. For this platform pitch correction was also not performed. The spread of the relative errors is representative of the relatively low camera height.

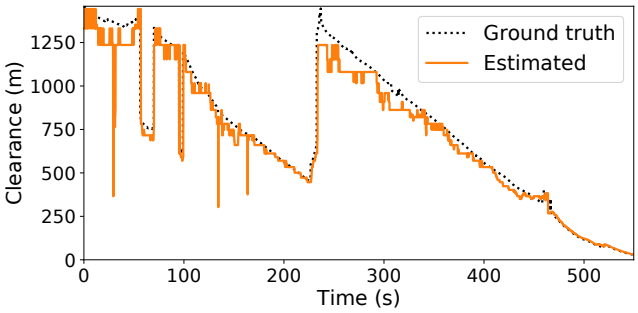

Fig. 6: Water clearance distance for route Helsinki B.

D. Route Helsinki B

In this route Suomenlinna II is approaching the Market Square in Helsinki.

In Fig. 4a the clearance lines intersect a small island with bearing $155°$ and a navigation pole with bearing $205°$. Both elements are also visible on the map view. In Fig. 4b the line at bearing $205°$ reaches another vessel in navigation, which is also captured in the area clearance shown in the map view. In Fig. 4c the vessel is nearing the quay. As in the previous section, the area clearance appears to be over-estimated, possibly due to the vessel decelerating and the lack of pitch compensation. Notice that the jetty clearly visible at bearing $155°$ is not present in the charted land, but correctly captured in the area water clearance. This demonstrates an advantage of this technology compared to only relying on charts, which may be outdated at the time of use. In addition, the area clearance shows a hole between bearing $190°$ and $205°$, in correspondence of a docked vessel.

In Fig. 6 the estimated water clearance distance is compared with the chart-based ground truth. The clearance is estimated from 1.4 km until few tens of meters. The spikes in the estimated water clearance are caused by navigational poles which are correctly identified at a distance of almost 400 m. The quantized values of the estimated clearance visible for large distances, are representative of a single pixel in the image space.

Over the entire path traveled, the median relative error is 4.1%, with 5-th and 95-th percentile errors of -5.4% and 12.1%, respectively.

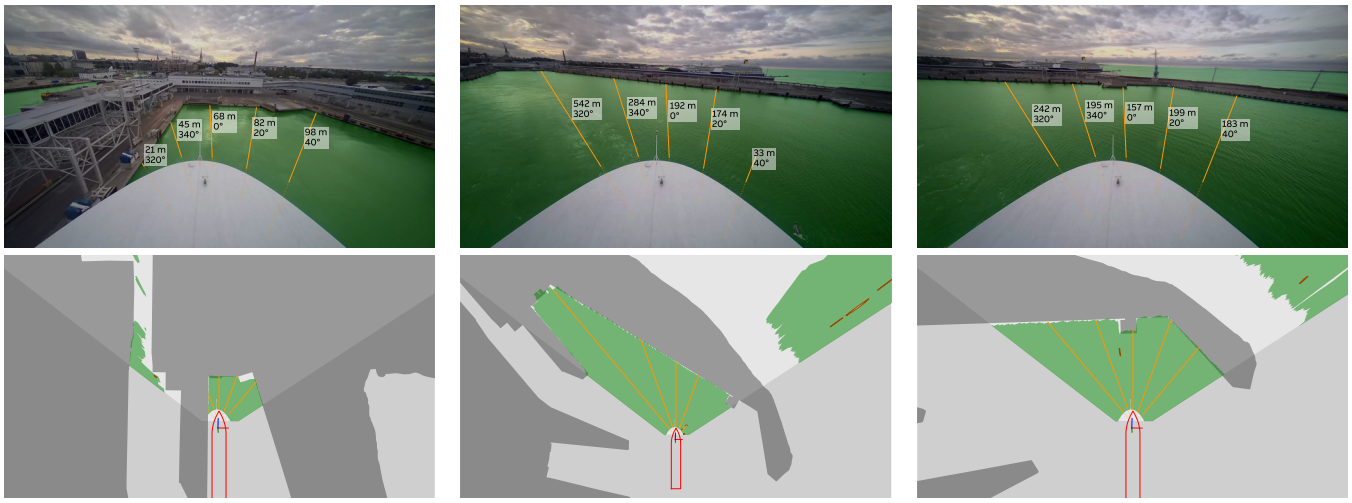

(a) $t = 114\,\mathrm{s}$ (b) $t = 392\,\mathrm{s}$ (c) $t = 464\,\mathrm{s}$

Fig. 7: Images for route Tallinn.

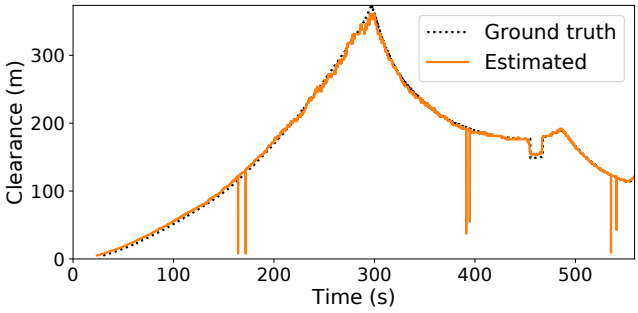

Fig. 8: Water clearance distance for route Tallinn.

E. Route Tallinn

In this section m/s Finlandia is leaving the harbor of Tallinn. The ship is docked bow first and while exiting the harbor, she reverses and makes a $180°$ turn within the harbor, cf. Fig. 7.

The estimated clearance along the centerline is compared with the ground truth in Fig. 8. In this sequence obstacles are up to 350 m away. At about $t = 300\,\mathrm{s}$, a discrepancy between the coastline chart and the water clearance is observed, which is due to a loading ramp that is not present in the charts. Furthermore, spikes in the estimated clearance are due to birds flying in front of the bow of the ship, c.f. Fig. 7b at bearing $40°$.

Over the entire path traveled, the median relative error is -0.2%, with 5-th and 95-th percentile errors of -19.1% and 2.6%, respectively. The small median error suggests a good calibration and a more favorable set up due to the higher camera position and relatively close distances to the quay. The large 5-th percentile error is due to the overestimation of the clearance distance in the initial part of the section, up until around 200 s. As visible in Fig. 7a, there is a quay structure extending above the water exactly along the central line clearance. This shows a limitation of the method in presence of obstacles above the water. By re-computing the percentiles starting at $t = 200\,\mathrm{s}$, the values change to -2.3%, 0.6%, 3.0%, for the 5-th, 50-th and 95-th percentile errors, respectively. This shows a significant improvement compared to the relative errors found in Sec. IV-C and IV-D, which is explained by the higher camera position and more stable platform.

V. CONCLUSIONS

In this work, we have presented a vision-based method for water clearance determination in maritime environments. We rely on a single camera to determine the area water clearance by using IMU pose-corrected back-projection. The water region in the image is found using semantic segmentation. From the area water clearance the water clearance distance is computed, i.e. the distance from the hull of the ego-vessel to the closest obstacle along a predefined direction. Both the area water clearance and the line water clearance are important to safe maneuvering and navigation. They can provide valuable input to the crew, or it can be used to further improve safety of autonomous operations.

Being reliant on a single camera, the proposed method requires accurate knowledge of the camera pose. A vision-based method [17] may be considered as a complement or alternative to the onboard IMU.

We validate the proposed approach using coastline charts and positions of the ego-vessel from an onboard GNSS receiver. Two different vessels were used for validation, and the method was shown to reliably estimate water clearances for distances beyond one kilometer. During a harbor maneuver it was shown that 90% of the relative errors were between $-2.3\%$and 3%.

It shown that the proposed method is able to detect land and quay structure as well as other obstacles. This reduces the dependency on sea charts for navigation, and the risks related to inaccurate sea charts. Other obstacles identified include navigational aid poles and other vessels.

REFERENCES

[1] J. Kim, C. Lee, D. Chung, and J. Kim, "Navigable area detection and perception-guided model predictive control for autonomous navigation in narrow waterways," *IEEE Robotics and Automation Letters*, vol. 8, no. 9, pp. 5456–5463, 2023.

[2] T. Huntsberger, H. Aghazarian, A. Howard, and D. C. Trotz, "Stereo vision–based navigation for autonomous surface vessels," *Journal of Field Robotics*, vol. 28, no. 1, pp. 3–18, 2011.

[3] H. Wang, Z. Wei, S. Wang, C. S. Ow, K. T. Ho, and B. Feng, "A vision-based obstacle detection system for unmanned surface vehicle," in *2011 IEEE 5th International Conference on Robotics, Automation and Mechatronics (RAM)*, 2011, pp. 364–369.

[4] H. Wang and Z. Wei, "Stereovision based obstacle detection system for unmanned surface vehicle," in *2013 IEEE International Conference on Robotics and Biomimetics (ROBIO)*, 2013, pp. 917–921.

[5] B. Bovcon, R. Mandeljc, J. Perš, and M. Kristan, "Stereo obstacle detection for unmanned surface vehicles by imu-assisted semantic segmentation," *Robotics and Autonomous Systems*, vol. 104, pp. 1–13, 2018.

[6] K. Kim and J. Kim, "Semantic segmentation of marine radar images using convolutional neural networks," in *OCEANS 2019 - Marseille*, 2019, pp. 1–6.

[7] W. He, X. Jiang, and G. Jin, "Rarws: A radar-assisted real-time water segmentation network to meet the autonomous navigation of usv in inland waterways," in *2022 26th International Conference on Pattern Recognition (ICPR)*, 2022, pp. 4168–4174.

[8] Y. Shan, X. Yao, H. Lin, X. Zou, and K. Huang, "Lidar-based stable navigable region detection for unmanned surface vehicles," *IEEE Transactions on Instrumentation and Measurement*, vol. 70, pp. 1–13, 2021.

[9] M. Keidar and G. A. Kaminka, "Efficient frontier detection for robot exploration," *The International Journal of Robotics Research*, vol. 33, no. 2, pp. 215–236, 2014.

[10] B. Bovcon and M. Kristan, "A water-obstacle separation and refinement network for unmanned surface vehicles," in *2020 IEEE International Conference on Robotics and Automation (ICRA)*, 2020, pp. 9470–9476.

[11] L. Žust and M. Kristan, "Temporal context for robust maritime obstacle detection," in *2022 IEEE/RSJ International Conference on Intelligent Robots and Systems (IROS)*. IEEE, 2022, pp. 6340–6346.

[12] L. Yao, D. Kanoulas, Z. Ji, and Y. Liu, "Shorelinenet: An efficient deep learning approach for shoreline semantic segmentation for unmanned surface vehicles," in *2021 IEEE/RSJ International Conference on Intelligent Robots and Systems (IROS)*, 2021, pp. 5403–5409.

[13] M. Sandler, A. Howard, M. Zhu, A. Zhmoginov, and L.-C. Chen, "MobileNetV2: Inverted residuals and linear bottlenecks," in *Proc. IEEE Conf. on computer vision and pattern recognition (CVPR)*, 2018, pp. 4510–4520.

[14] O. Ronneberger, P. Fischer, and T. Brox, "U-net: Convolutional networks for biomedical image segmentation," in *Int. Conf. on Medical image computing and computer-assisted intervention*, 2015, pp. 234–241.

[15] R. I. Hartley and A. Zisserman, *Multiple View Geometry in Computer Vision*, 2nd ed. Cambridge University Press, ISBN: 0521540518, 2004.

[16] S. Suzuki and K. be, "Topological structural analysis of digitized binary images by border following," *Computer Vision, Graphics, and Image Processing*, vol. 30, no. 1, pp. 32–46, 1985.

[17] S. Singhal, Y. Ao, D. Maas, B. Arsenali, and S. Maranò, "Marine vessel attitude estimation from coastline and horizon," in *2023 IEEE/RSJ International Conference on Intelligent Robots and Systems (IROS)*, 2023, pp. 6149–6154.